Journal of Power Sources 195 (2010) 4685–4694

Contents lists available at ScienceDirect

Journal of Power Sources

journal homepage: www.elsevier.com/locate/jpowsour

Optimizing the mass transport phenomenon around micro-electrodes of an enzymatic biofuel cell inside a blood artery via finite element analysis method

Yamini Parikh, Jung-Hoon Yang, Chunlei Wang*

Department of Mechanical and Materials Engineering, Florida International University, 10555 W. Flagler Street, Miami, FL 33174, USA

ARTICLE INFO

Article history:
Received 21 December 2009
Received in revised form 26 January 2010
Accepted 27 January 2010
Available online 20 February 2010

Keywords:
Enzymatic biofuel cell
Finite element analysis
Mass transport

ABSTRACT

Two different orientations of an enzymatic biofuel cell (EBFC) chip, involving highly dense and three-dimensional cylindrical micro-electrodes arrays, have been studied with the finite element method. Mass transport phenomenon around the micro-electrodes of an EBFC chip inside a blood artery has been simulated. The stability of the chip to its position and blood flow pattern surrounding it are also investigated. The comparison between horizontal position (HP) and vertical position (VP) reveals that the chip can be more stable in VP rather than in HP. In VP, the diffusive flux and convective flux values are bigger compared to HP, but both these fluxes are non-uniform around all electrodes in both the positions. In addition to that in case of HP, the electrodes located at different positions on a chip receive different amount of glucose. A novel designed chip with holes through the substrate has enhanced the diffusive and convective flux in the HP of a chip and also all micro-electrodes on a chip receives similar amount of glucose uniformly throughout from the top to the bottom.

1. Introduction

Since the 1950s, numerous active implantable medical devices (IMDs) [1–6], such as pacemakers, defibrillators, cochlear implants, neuro-stimulators, artificial hearts, and drug delivery systems, have been developed. Effective functionality of these IMDs mainly depends on the continuous supply of electricity. Traditional power sources for these implants are lithium primary or lithium ion secondary batteries [7,8]. Despite of abstract estimations that batteries would last for at least 5 years, the major complications were found that the battery at body temperature and at nominal load will not last much beyond 2 years because of all types of issues, such as internal short circuits, inefficient components, and encapsulation problems [9]. Because of the challenges associated with batteries, researchers recently paid considerable attention towards biofuel cells (BFCs). The use of natural biological fuels, such as glucose or fructose, abundantly available inside a human body; operation at physiological condition of pH 7, body temperature 37 °C and normal body pressure 80–120 mmHg; and also biocompatibility make BFCs very promising to be used as implantable power sources [2]. Currently, researchers are mainly focusing on enzymatic biofuel cell (EBFC) instead of microbial fuel cell (MFC), because enzymes have higher volumetric catalytic activity compared to microbes [10,11], and also 'selective' nature of enzymes gives an opportunity to miniaturize the device by removing expensive and bulk membranes [3,4].

Until now, majority researches are focused on in vitro experiments by mimicking physiological conditions. The additional complex problems may arise when a BFC chip is placed inside a blood artery. The first is with implantation process itself, which involves a surgery for the insertion of a BFC, electrical wires and other necessary electronics components. The second is the stability of this chip inside an artery and how/where this chip can be fixed such that it can survive against the blood flow. Third problem is the clotting of the blood. This chip should be placed in such a way that it must not obstruct the flow of blood and must not even lead to substantial pressure drop inside an artery, which can be dangerous to a human health. The fixation of this chip with the blood artery also should not harm the blood vessel walls.

In order to improve mass transport around micro-electrodes by optimizing the positioning of an EBFC chip, we have adopted the finite element analysis (FEA) approach. While achieving this goal, we also look into the stability of an EBFC inside a blood artery. FEA is a powerful tool to mimic the behavior of an EBFC chip performance inside an artery. We use COMSOL 3.5 Multiphysics software to analyze mass transport for different orientations of an EBFC chip inside a blood artery. On the initial stage, we have analyzed only two orientations: horizontal position (HP) and vertical position (VP). The stability of the chip in these positions, diffusion and convectional fluxes around micro-electrodes has been finely investigated. We have proposed a novel chip design, with holes in between all electrodes on the substrate, which can drastically improve the diffusion

* Corresponding author. Tel.: +1 305 348 1217; fax: +1 305 348 1932.
E-mail address: wangc@fiu.edu (C. Wang).

0378-7753/$ – see front matter © 2010 Elsevier B.V. All rights reserved.
doi:10.1016/j.jpowsour.2010.01.064

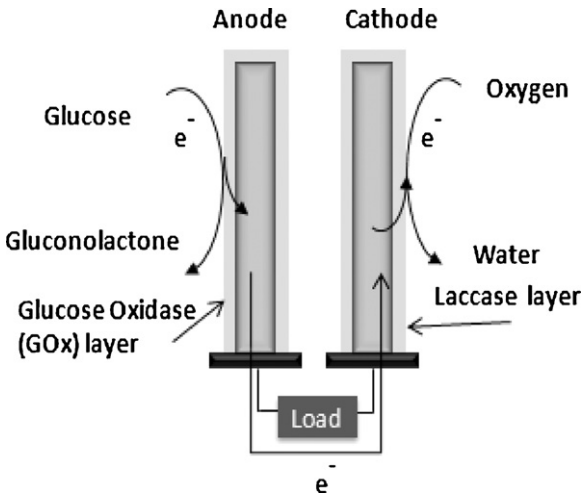

Fig. 1. Schematic of an EBFC reaction mechanism.

in between micro-electrodes. Its comparison with the conventional HP chip design is also elucidated in this paper.

2. Theory

2.1. EBFC redox reaction mechanism

Fig. 1 depicts the mechanism of an EBFC with glucose oxidase immobilized on anode and laccase immobilized on cathode. The EBFC utilizes the chemical energy, entrapped into bio-molecules (e.g. glucose, sucrose, etc.), and convert it to electricity. The redox reaction occurs catalytically by enzymes, immobilized onto electrodes. Glucose oxidase (GOx) reacts with glucose ($C_6H_{12}O_6$) and produces gluconolactone ($C_6H_{10}O_6$) and hydrogen peroxide [2,12,13]. The hydrogen peroxide is oxidized on anode and generates electron and hydrogen ions. The electrons travel through anode to cathode via external load and produce electric current. On cathode, dissolved oxygen is reduced via laccase and generates water by combining electrons and hydrogen ions. Water is the only byproduct from this reaction, which provides clean energy.

2.2. Michaelis–Menten enzyme kinetics

In this study, glucose is the only substrate considered and hence the simulation study is restricted to single substrate enzyme kinetics theory. The Michaelis–Menten [14] kinetic model of a single-substrate reaction is the basis for most single-substrate enzyme kinetics:

$$V_0 = \frac{V_{\max} \times [S]}{K_M + [S]} \quad (1)$$

where [S] is substrate concentration, V_0 is the reaction rate of enzymes, and $V_{\max}$ is the enzyme's maximum reaction rate.

3. Computational modeling

In order to simulate the behavior of an EBFC inside an artery, mainly two physics have been coupled: (1) the pressure and velocity of glucose flow inside an artery, and (2) total flux of glucose around the micro-electrodes.

3.1. Computational domain

The schematic of a prototype model of an EBFC chip, having three dimensional, highly dense micro-electrode arrays is shown in Fig. 2a. General dimensions of the chip which can be easily fabricated by C-MEMS fabrication technologies are considered in the simulation geometry [15]. Height of all electrodes is 300 μm, diameter is 30 μm, distance between two electrodes (well width) is 40 μm and enzyme layer thickness is 10 μm. With these electrode dimensions and foot print area of 2 mm^{-2}, 12 pairs of electrodes can be accommodated in one row on a chip. Two-dimensional view of an EBFC chip is considered as simulation geometry. Current collectors are assumed to be placed at the bottom of all electrodes and on the insulation layer. This EBFC chip is assumed to be centrally placed inside a blood artery with diameter of 1.5 cm [16]. In the proposed design (Fig. 2b), holes are provided on the SiO_2 layer in between all anodes and cathodes. The diameter of holes in our design is 20 μm, but it can be varied depending upon the well width.

3.2. Computational cases

In this paper, two cases have been considered. In the first case, the comparison has been made between the chips with distinct orientations—HP (Fig. 2c) and VP (Fig. 2d), inside an artery. In the second case, the comparison has been made between chips with and without holes in HP. In both these figures, IN represents the inlet of an artery and OUT represents the outlet of an artery. In the HP, all the electrodes on a chip are facing towards inlet of an artery, while in VP, all the electrodes are facing the artery wall. For the initial stage studies of the orientations, these can be very good approximate positions of a chip inside an artery. The *X*-axis and *Y*-axis are shown in the figures, to cleary mention the position of electrodes while analyzing and discussing the graphs. In both HP and VP (0,0) is the center of the chip at the top surface of a SiO_2 layer. The ±*X*-axis is going from center of a chip to the right and left artery walls, respectively, and ±*Y*-axis is going from bottom of an electrode to the inlet and outlet of an artery, respectively. The blood artery walls are assumed to be rigid and straight.

3.3. Subdomain materials and properties

Here, the electrodes are consisted of an array of glassy carbon electrodes on a silicon substrate with oxide layer as insulator layer. For simplicity, GOx is considered on all electrodes uniformly. The constant parameters related to simulation are shown in Table 1.

3.4. Governing equations and boundary conditions

We use (1) the diffusion and convection application module, which solves Fick's law:

$$\delta_{ts}\frac{\partial c}{\partial t} + \nabla \cdot (-D\nabla c) = R - u \cdot \nabla c \,(\text{non-conservative}) \quad (2)$$

where δ_{ts} is the time scaling co-efficient; c is the concentration of species (mol m^{-3}); D is the diffusion co-efficient (m^{-2} s); and R is the reaction rate (mol m^{-2} s^{-1}); and u is the velocity field (m s^{-1}); and (2) incompressible Navier–Stokes application module, which

Table 1
Constants and parameters for simulation modeling.

Constant	Value
Universal gas constant	8.314 J mol^{-1} K^{-1}
Body temperature	300 K
Faraday's constant	96,485 C mol^{-1}
Diffusion co-efficient of glucose	7e−10 m^2 s^{-1} [17–19]
Michaelis–Menten constant for GOx	0.383 mM [20]
Maximum reaction rate of GOx	0.731 mM min^{-1} [20]
Blood density	1060 kg m^{-3} [21]
Blood viscosity	0.005 Pa s [22]

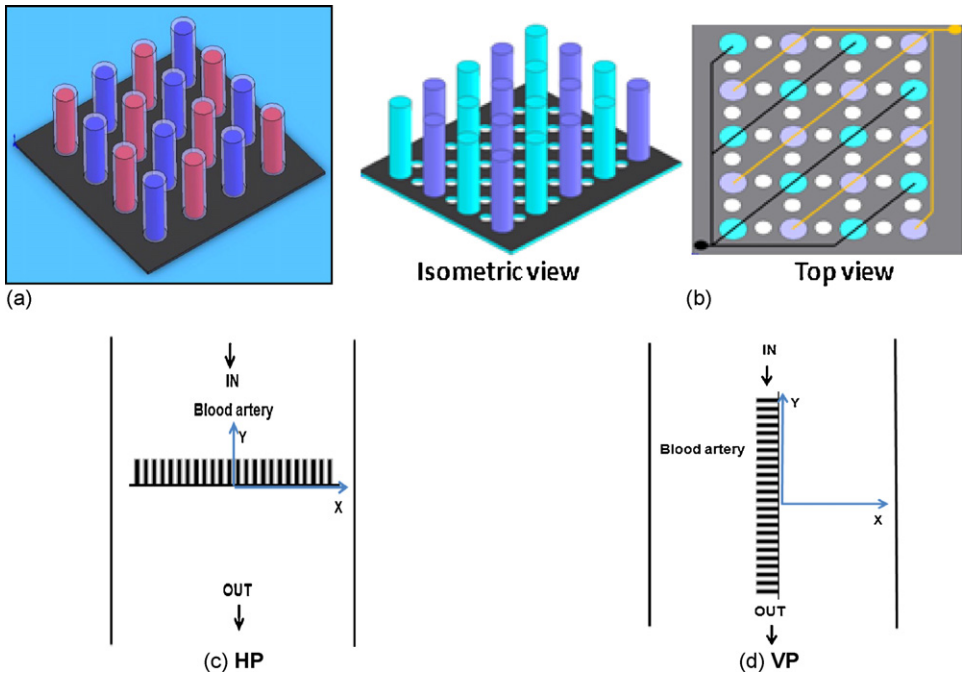

Fig. 2. (a) Schematic diagram of a prototype EBFC chip, with anodes and cathodes alternately arranged. The transparent layers around electrodes show the enzyme layers. (b) Schematic of a proposed design of a chip with holes in the substrate: isometric view (left) and top view (right) with anodes and cathodes collectors. Simulation geometries showing orientation of a chip inside an artery in: (c) horizontal position (HP) and (d) vertical position (VP).

solves Navier–Stokes pressure/velocity and continuity equations:

$$\rho\frac{\partial u}{\partial t} - \nabla\cdot[\eta(\nabla u + (\nabla u)^T)] + \rho(u.\nabla)u + \nabla p = F \quad (3)$$

where η is the dynamic viscosity (Pa s); ρ is the density of a fluid (kg m^{-3}); u is the velocity field (m s^{-1}); p is the pressure (Pa); and F is a volume force field such as gravity. Boundary conditions for diffusion and convection module, and Navier–Stokes application module are shown in Table 2.

The pressure variation in each cardiac cycle is considered with a simple trigonometry function (fluid structure interaction in a network of blood vessels model, COMSOL Multiphysics), plotted in Fig. 3, to maintain normal systolic/diastolic pressure variation of 120/80 mmHg in the artery [24,25]. The glucose amount flowing in the artery will also change at the inlet according to contraction and extraction of blood artery. To show the effect of varying amount of glucose, the MFC is multiplied with glucose concentration at the artery inlet to consider continuously varying glucose flux.

Table 2
Boundary conditions for diffusion and convection and Navier–Stokes application modules.

Boundary	Condition
(1) Diffusion and convection application module	
Anode–enzyme layer interface and cathode–enzyme layer interface	Zero inward flux
Enzyme layers–bulk interface	Continuity
Inlet of an artery	Inward flux = 5 mM [23]
Outlet of an artery	Convective flux
SiO_2 layer boundaries	Insulation
(2) Navier–Stokes application module	
Anode–enzyme layer interface and cathode–enzyme layer interface	Wall–no slip
Enzyme layers–bulk interface	Continuity
Inlet of an artery	Inlet pressure
Outlet of an artery	Outlet—no viscous stress
SiO_2 layer	Insulation

4. Results and discussions

4.1. Comparison between two orientations

In this section, case I for the comparison between an EBFC chip in HP and VP has been inferred.

4.1.1. Pressure and velocity distribution around an EBFC

Pressure distribution around the chip is shown in Fig. 4a for HP and in Fig. 4b for VP. In Fig. 4a, there is a broad region of high pressure (approximately 112.51 mmHg) above the chip and low pressure (112.47 mmHg) below the chip. There is an abrupt change in the pressure above and below the chip and this pressure gradient above and below the chip may exert downward force on a chip which may push down a chip from its position. In Fig. 4b, with the chip placed vertically, the pressure is highest at only front corners of the chip, while almost uniform around all electrodes. The pressure

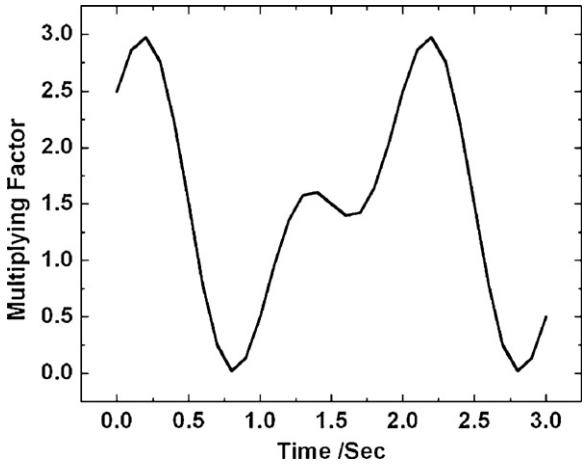

Fig. 3. Trigonometry function for pressure variation.

is 112.56 mmHg at the front corners and 112.48 mmHg around all other electrodes. The wide high pressure region in the HP of a chip is due to a higher angle of attack due to chip in a way of glucose flow. The whole foot print area of the chip is exposed to the incoming flow of glucose in case of HP. In case of VP, the angle of attack is very small because only one side of the top most electrodes on a chip is exposed to the incoming flow of glucose.

The velocity profiles are depicted in Fig. 4c and d, for the HP and VP of a chip inside an artery, respectively. In both these profiles, it can be observed that there are zero velocity layers—'boundary layers' near the solid surfaces, such as blood vessel wall and chip surfaces. The glucose right next to the solid edges sticks to the surfaces due to frictional interaction of glucose with surfaces. In both the cases the glucose is ideally following parabolic pattern of flow. The fluid velocity is higher at the center of the artery in both the cases while the glucose layers nearer to the solid walls slow down gradually, and come to a complete stop exactly at the walls. These boundary layers start forming at the beginning of the flow, and then gradually and slowly becoming thicker. The velocity values simulated here are also comparable with other simulation results [26,27].

In addition, the surface plot of Navier–Stokes pressure along with the velocity streamlines for the HP and VP of a chip is achieved as shown in Fig. 4e and f, respectively. In HP of a chip (Fig. 4c and e), the flow around the chip is unsteady as the direction and speed of glucose is different at each point in the flow. In VP of a chip (Fig. 4d and f), the flow is more steady as the direction and speed of a flow remains constant at any point in the space (although not same velocity at all points in the fluid). In case of an HP, small vortices are formed under the chip, which is not the case in VP. The reason for the formation of small turbulences under the chip in HP is due to boundary layers separation, as shown in Fig. 4e. There is an abrupt change in the direction of a flow due to the object in way of glucose, but the glucose layers, just next to the chip surfaces, are unable to make a sudden change in their flow direction, and stay with the solid surfaces. Therefore, the boundary layers get detached from the chip, and a region of low pressure turbulence forms under the chip. This results in the wide wake region, with zero velocity, below the chip, which can be observed. This wake region causes the pressure drag on the chip which may eventually lift up the chip. Fig. 4f shows the velocity profile around the vertical positioned chip. Unlike the HP, the wide wake region surrounding the chip is not formed. Here the flow is steady without any turbulence compared to the flow in HP. All the streamlines are almost parallel i.e. the flow is laminar. The sudden pressure change above and below the chip, and 'wake' region formation below the chip,

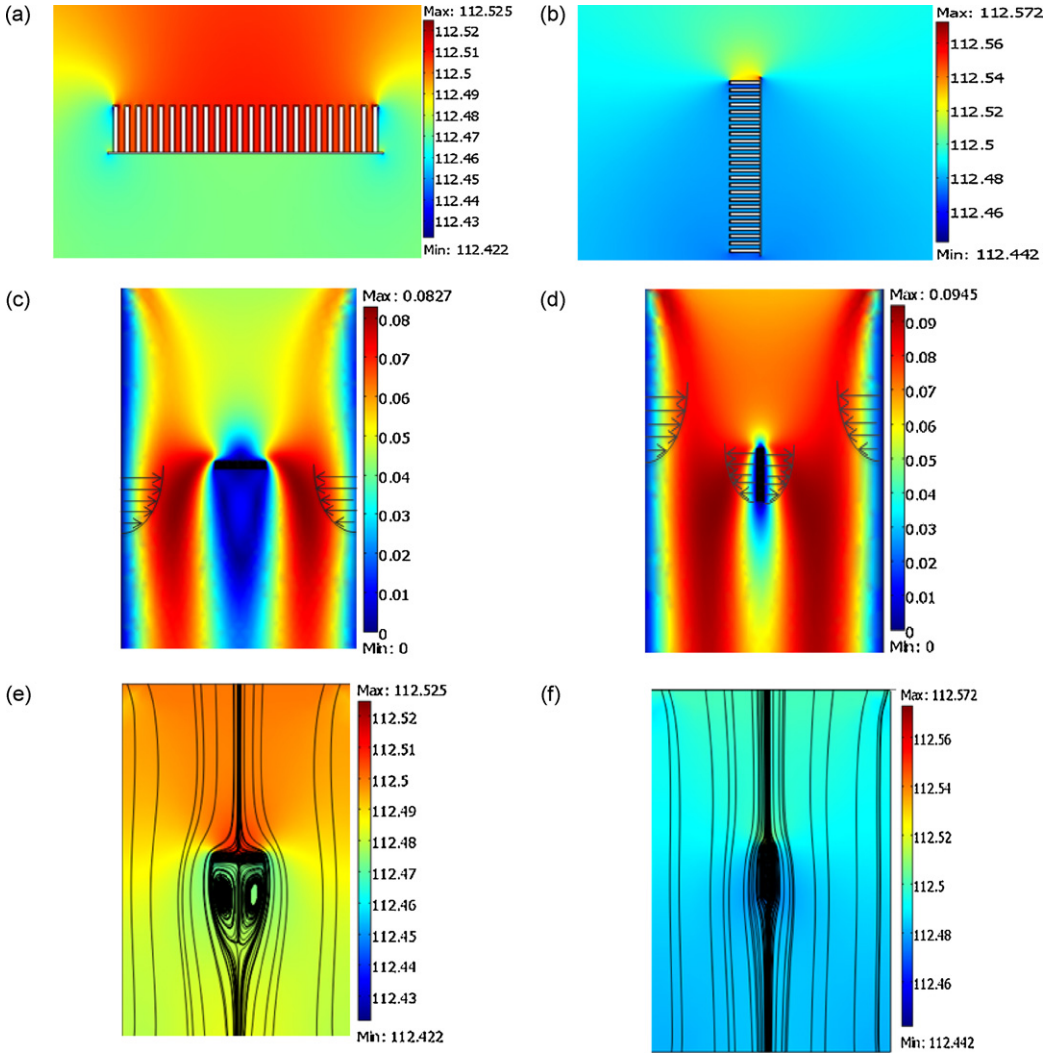

Fig. 4. Simulation profiles of Navier–Stokes pressure distribution around (a) HP and (b) VP of a chip. Surface plot of Navier–Stokes velocity distribution around electrodes: (c) for the HP and (d) for the VP of a chip inside blood artery. Surface plot of Navier–Stokes pressure and streamlines for velocity distribution around electrodes: (e) for HP of a chip, and (f) for VP of a chip inside blood artery.

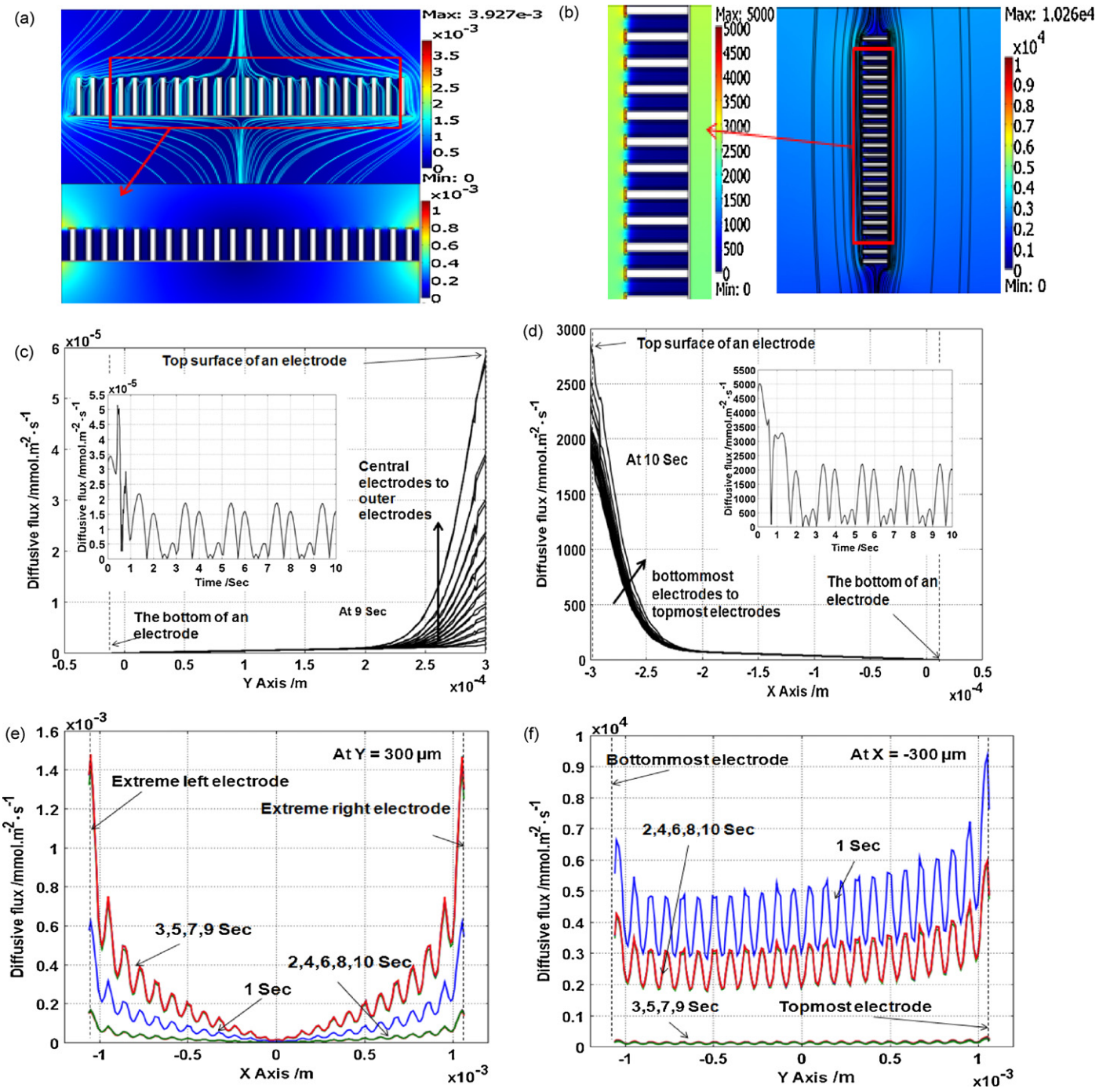

Fig. 5. Surface plot with streamlines for diffusive flux of glucose around micro-electrodes for (a) HP and (b) VP. Diffusive flux, in between all 24 electrodes from bottom of electrodes to up to 300 μm height is shown for (c) HP and (d) VP. Diffusive flux at top of all the electrodes from left most to right most electrodes for 0–10 s is shown in (e) HP and (f) VP.

render instability to the chip in horizontal position. For this reason, the extra care must be incorporated while fastening the chip in horizontal such that it does not flow away from its original position in the artery.

4.1.2. Glucose flux around an EBFC electrodes

The diffusive flux, convective flux and total flux surrounding micro-electrodes in the blood artery have been analyzed for both horizontal and vertical positions in order to understand in which position maximum glucose can reach to all micro-electrodes.

4.1.2.1. Diffusive flux profile. Diffusive flux defines the amount of glucose flowing through the small area during a small time interval, and it is driven by concentration gradient solely. The diffusion in between micro-electrodes has been minutely inspected in Fig. 5, where Fig. 5a and b shows the simulation profiles for diffusive flux along with the streamlines around micro-electrodes in HP and VP, respectively. In the insets of both the figures, it is seen that the diffusive flux is very less in between electrodes compared to the surrounding bulk regions. In HP, it is observed that the diffusive flux is less near the central electrodes and increasing while going towards outer electrodes. However, the diffusive flux is almost same on top of all electrodes in VP. In both the position cases, the

diffusive flux is following laminar pattern. Fig. 5a and b has been graphically represented in Fig. 5c–f, where Fig. 5c and e is for HP and Fig. 5d and f is for VP. The diffusive flux from bottom of an electrode to top of an electrode is investigated in HP and VP as shown in Fig. 5c and d, respectively. The diffusive flux in HP (Fig. 5c) shows that till the 200 μm height of electrodes the glucose flux is negligible, while it is increasing afterwards and becoming almost 0.1×10^{-5} to 6×10^{-5} mmol m^{-2} s^{-1} at the top. The flux is not uniform from central to outer electrodes. The electrodes located at the circumference of a chip are having more flux compared to those located in the center of the chip. The variation of the diffusive flux distribution around inner to outer electrodes is high in HP. This is also evident from Fig. 5e, which shows the diffusive flux at the top of all electrodes in HP. The value of extreme left and right electrodes is 1.5×10^{-5} mmol m^{-2} s^{-1}, while at the center it is almost negligible. In Fig. 5d, the graph shows the diffusive flux of glucose around all electrodes from top to bottom, in VP. Here, it is observed that the flux is almost negligible in between electrodes up to 200 μm height and after that it is increasing to almost 2000–3000 mmol m^{-2} s^{-1}. In this position, the diffusive flux is higher at the topmost electrodes and decreases to the bottommost electrodes. This is also noticed in Fig. 5f, where the diffusive flux at the top of all electrodes is shown in VP. At bottommost electrodes on a chip is having lesser diffusive flux compared to topmost electrode. The diffusive flux is almost

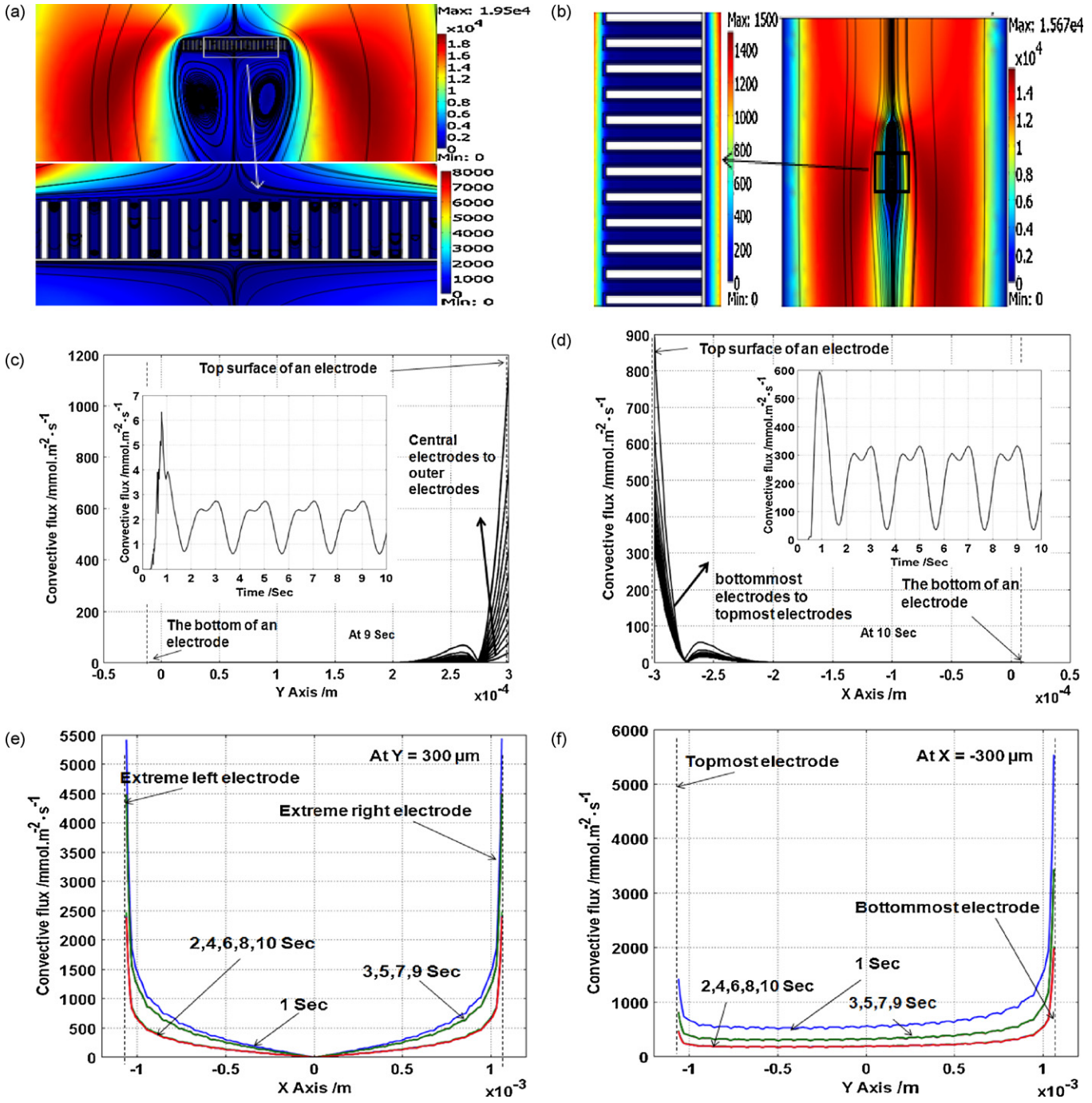

Fig. 6. Surface plot with streamlines for convective flux of glucose around micro-electrodes for (a) HP and (b) VP, convective flux in between all 24 electrodes from bottom of electrodes to up to 300 μm height is shown for (c) HP and (d) VP, convective flux at top of all the electrodes from leftmost to right most electrodes for 0–10 s in (e) HP and (f) VP.

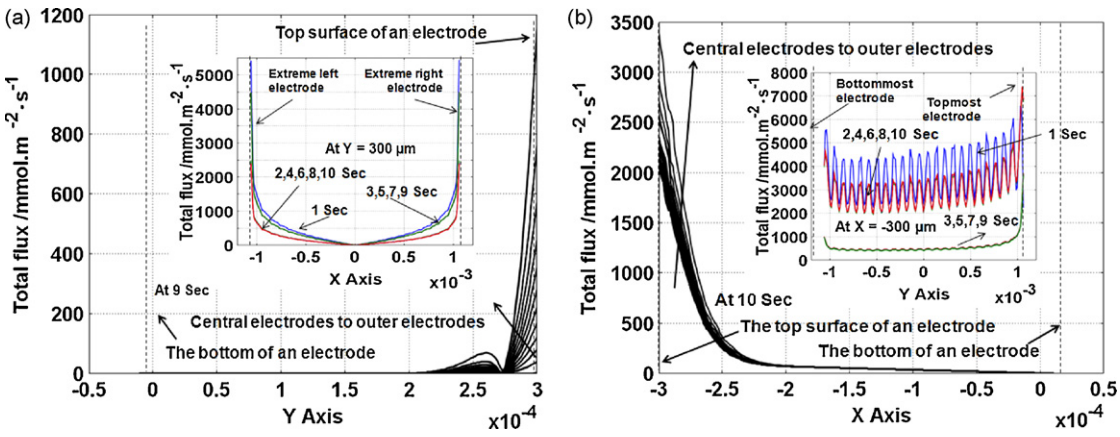

Fig. 7. Total fluxes in between micro-electrodes for (a) HP and (b) VP. Insets provide the total flux on top of all electrodes.

3000 mmol m^{-2} s^{-1} at the bottommost and then gradually increasing to 4000 mmol m^{-2} s^{-1} at the topmost electrode on the chip. In both Fig. 5c and d, the inset figures show the variation of diffusive flux for up to 10 s. The flux is not constant at every instance, but it is oscillating as shown in inset figures. The diffusive flux profiles in these figures are considered at the time, when the flux reaches its maximum value. The ripples in the diffusive flux in Fig. 5e and f are observed, because the flux is higher exactly at the top of electrodes while lesser in the vicinity between any two electrodes. In comparison of HP and VP, the diffusive flux is 8 orders larger in case of VP than in HP.

4.1.2.2. Convective flux. When a chip is placed in the artery where the fluid is having its own convection, then the mass transfer is not only dominated by concentration gradient but it also depends on the convection of the moving fluid surrounding it. In this study, the convective flux, i.e. convective mass transfer has been driven by velocity of the glucose generated due to heart pumping. The forced convection of an incompressible glucose (blood in reality) flow in the artery majorly affects the mass transport around the micro-electrodes in this situation. The surface plots of convective flux with streamlines are shown for HP and VP in Fig. 6a and b, respectively. It is clearly evident that the convective flux patterns

Table 3
Comparison of diffusive flux and convective flux in the EBFC chip with and without the holes.

Property	Proposed design (with holes)	Prototype design (without holes)
Diffusive flux streamlines surrounding the chip in the artery	Fig. 8a: All the streamlines for diffusive flux are parallel. The flow is taken place through the holes in between micro-electrodes.	Fig. 5a: All the streamlines are diverging at the top of the electrodes and is diverted to the side of a chip.
Diffusive flux near the holes	Fig. 8a: There is a sharp increase in the diffusive flux (venture effect) in the holes. At the holes the diameter is reducing and hence the velocity of the flow increases. Therefore, the diffusive flux increases.	Fig. 5a: There is no hole and hence there is no sharp increase in the diffusive flux.
Diffusive flux in between micro-electrodes	Fig. 8c: The diffusive flux has been drastically improved in between micro-electrodes. The diffusive flux is about 3500 mmol m^{-2} s^{-1} from top to bottom of all electrodes.	Fig. 5c: The diffusive flux is negligible up to 200 μm height and then it is approximately $0–6 \times 10^{-5}$ mmol m^{-2} s^{-1}, which is significantly less compared to the proposed design.
Diffusive flux uniformity	Fig. 8e: The diffusive flux is uniform around all electrodes. That means all the electrodes get similar amount of glucose at every instance.	Fig. 5e: The diffusive flux is non-uniform with negligible flux at the central electrodes, while increasing towards outer electrodes. All the electrodes gets different amount of glucose flux.
Convective flux surrounding chip	Fig. 8b: There is a random flow below the chip due to small vortices.	Fig. 5b: There is a random flow below the chip.
Convective flux in between electrodes	Fig. 8d: From bottom to up to 25 μm height of electrode that velocity is decreasing from 175 to 70 mmol m^{-2} s^{-1} and it stays at almost 70 mmol m^{-2} s^{-1} up to 275 μm height and then increasing until the top of electrodes.	Fig. 5d: Convective flux is negligible in between electrodes up to 275 μm heights and then increasing up to 500–1000 mmol m^{-2} s^{-1}.
Convective flux at top of all electrodes	Fig. 8f: The convective flux at the top of all electrodes is not exactly same for all electrodes. It is increasing from central electrodes to outer electrodes.	Fig. 5f: The uniformity at the top of all micro-electrodes is same as proposed design.
Total flux in between electrodes	Fig. 9a: Total flux remains about 3500–4000 mmol m^{-2} s^{-1} in between all electrodes.	Fig. 7a: Total flux is negligible in between all electrodes up to 275 μm height of electrodes and then increasing. It varies from 0 to 1200 mmol m^{-2} s^{-1} for central to outermost electrodes.
Total flux at top of all electrodes	Fig. 9b: Total flux is uniform for all electrodes.	Fig. 7a: Total flux is not uniform on top of all electrodes. Highest on top of circumferential electrodes and decreases towards central electrodes.

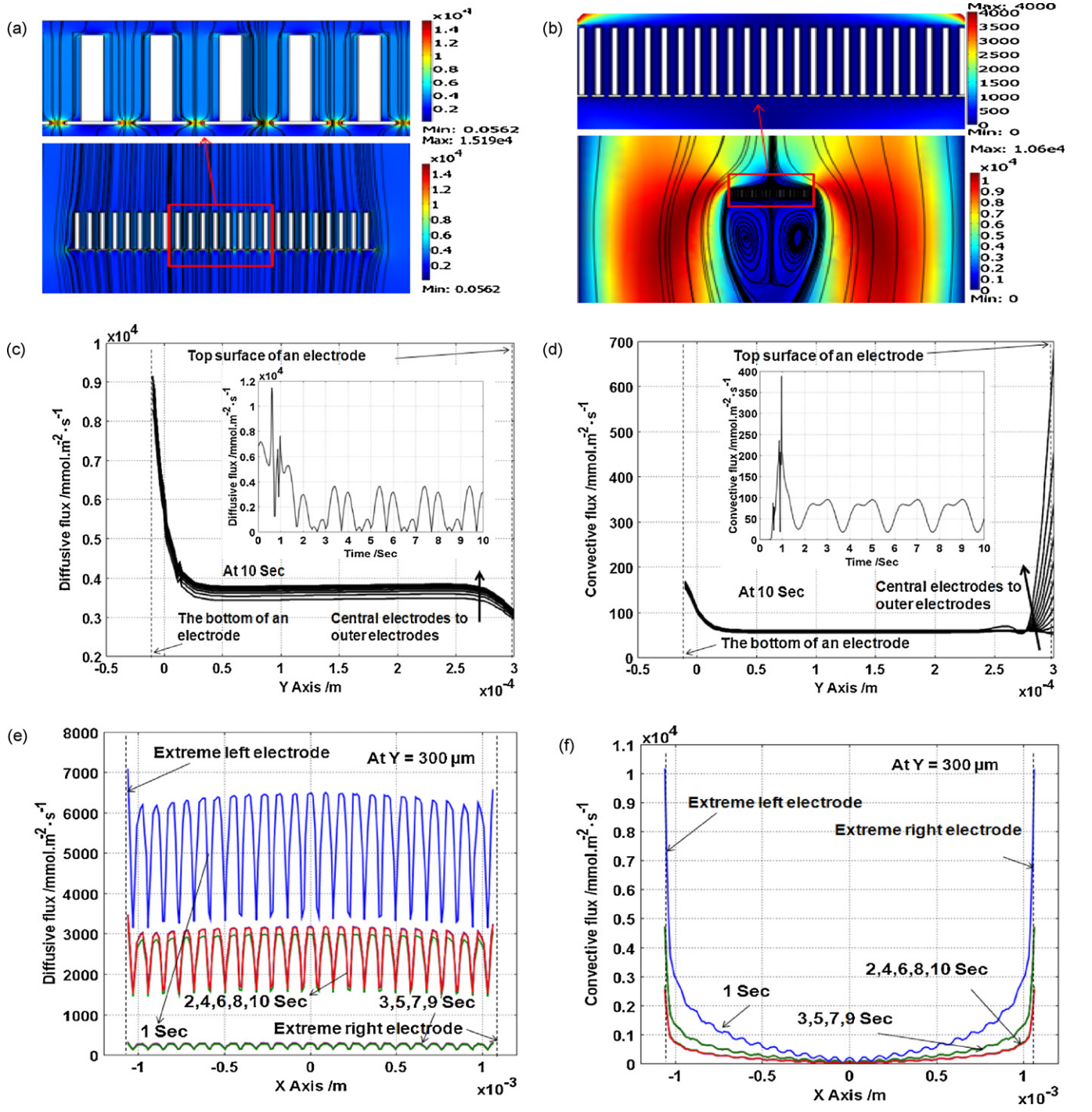

Fig. 8. Surface plot with streamlines for (a) diffusive flux and (b) convective flux of glucose around micro-electrodes with holes through the substrate. (c) Diffusive flux and (d) convective flux in between all 24 electrodes from bottom of electrodes to up to 300 μm height; (e) diffusive and (f) convective flux at top of all the electrodes from leftmost to right most electrodes for 0–10 s.

follow the velocity profile. The comprehensive graphical analysis has been given in Fig. 6c and d, for HP and VP, respectively. In both the graphs, it is evident that the convective flux is very less in between micro-electrodes for up to 250 μm of height and then it is increasing. That means the glucose has negligible convective motion in between electrodes. In HP, the convective flux at the top is around 1200 mmol m^{-2} s^{-1} on extreme ends electrodes, while it is reducing and becoming negligible at the central electrodes. The glucose tries to flow away from both sides of a chip. In VP, the flux is decreasing from topmost electrode to bottommost electrodes on the chip. The flux at the bottommost electrode is about 300 mmol m^{-2} s^{-1}, while that at the topmost electrode is around 900 mmol m^{-2} s^{-1}. This is also evident from Fig. 6e and f, respectively for HP and VP. At any instance, the flux is non-uniform in HP as well as VP.

4.1.2.3. Total flux. Total flux is the combination of a diffusive flux and a convective flux. Fig. 7 depicts the total flux data for (a) HP and (b) VP of a chip. In HP, flux is negligible up to almost 275 μm height of electrodes and then increasing at the top. Total flux is highest at the top of outer most electrodes (about 1200 mmol m^{-2} s^{-1}) and then reducing to the central electrodes

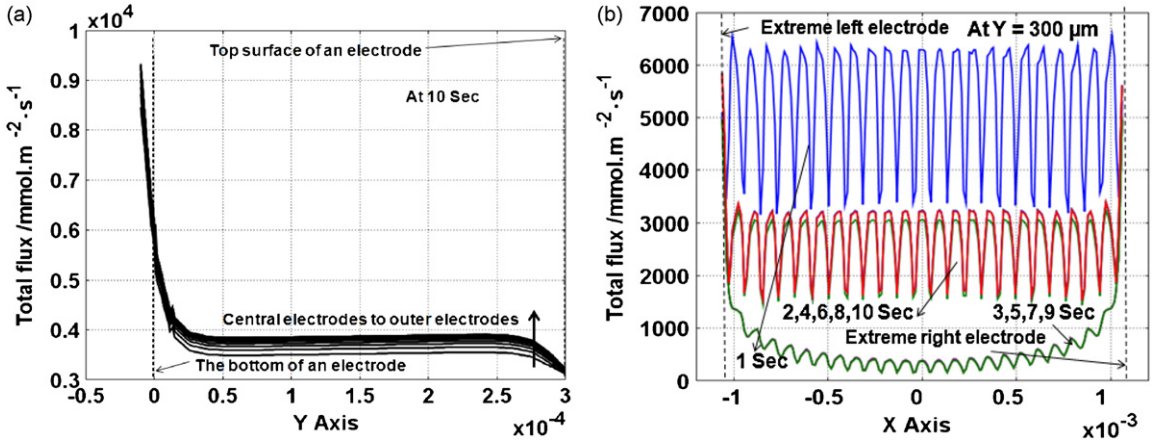

Fig. 9. For a proposed design of a chip with holes in substrate. (a) Total flux in between all micro-electrodes and (b) total flux on top of all electrodes.

(approximately 0 mmol m^{-2} s^{-1}). In case of VP, the flux is almost uniform on top of all electrodes, with negligible value in between electrodes up to 200 μm height and then gradually increasing to about 2000–3500 mmol m^{-2} s^{-1} at the top of all electrodes.

4.2. Comparison of a novel design with the prototype design in HP

Here, in the case II, the new design with the holes (Fig. 2b) in between all micro-electrodes has been inspected precisely and compared with the prototype design (Fig. 2a). The diffusive flux (Fig. 8a, c, e) and convective flux (Fig. 8b, d, f) profiles for the new design are compared with diffusive flux (Fig. 5a, c, e) and convective flux (Fig. 7a, c, e) profiles of the prototype model, respectively. The streamlines present the lines of motions of glucose at a particular instance. The comparison between a chip with holes (proposed design) and without holes (prototype design) is described in Table 3.

From Table 3, it is inferred that the total flux (combined diffusive and convective flux) has been improved in between all micro-electrodes in terms of values and their uniformity for the chip with the holes. This enhanced mass transport around micro-electrodes is significantly important for an EBFC performance. This proposed design can also be advantageous to prevent blood clotting. Human blood is mainly consisted of red blood cells and white blood cells. The sizes of all these cells such as red blood cells (6 μm), lymphocyte (7–8 μm), neutrophil (10–12 μm), eosinophil (10–12 μm), basophil (12–15 μm), and monocytes (14–17 μm) are mostly smaller than 20 μm, the size of the holes provided in the chip [28]. So these cells can pass through the holes in between micro-electrodes without blocking the way in between micro-electrodes. These holes can be made bigger depending on the requirement. The improved convection in between micro-electrodes may also be forceful enough to eliminate the bubble formation. However, the biomechanical process and hemodynamic process are more complex than convection and diffusion, especially on the micro-scale level. Cell growth and clotting phenomenon are related to many aspects, such as: biocompatibility, bending of blood artery, platelet and protein components. More detailed research needs to be done with biologists in order to obtain more sufficient and helpful information and further reach the applicable level of the EBFCs.

5. Conclusions

From the comparison between HP and VP of a chip without holes, we can conclude that the chip can be more stable in the vertical position as there is no external drag forces due to turbulences surrounded the chip. The diffusion in between micro-electrodes is negligible in horizontal position and it is better in vertical position of a chip. In HP, the flux distribution is very different for each electrode from center to edge. The diffusive flux and convective flux are higher for micro-electrodes located on the circumference of the horizontally positioned chip. At the central electrodes, these fluxes are negligible. In VP, these fluxes are uniform for all electrodes although negligible in between electrodes. In VP, there will not be limitation of increasing the foot print area. In HP, an increase in foot print area will allow thicker boundary layers to be formed, which can obstruct the blood flow. From the comparison between a prototype design without holes and a proposed design with holes, we can conclude that the diffusive flux and convective flux have been drastically improved in a chip with holes. The uniformity of these fluxes has also been improved with all micro-electrodes receiving similar diffusive and convective flux. The overall flux has been drastically improved in HP with holes compared to a chip without holes in both horizontal and vertical position.

Acknowledgements

This project is supported by National Science Foundation (CBET# 0709085). We would like to thank Dr. Marc Madou at University of California Irvine, Dr. Sylvia Daunert at University of Kentucky, Dr. Jiuhua Chen and Dr. Norman Munroe at Florida International University for useful discussion.

References

[1] D. Ivnitski, B. Branch, P. Atanassov, C. Apblett, Electrochem. Commun. 8 (2006) 1204–1210.
[2] X. Wei, J. Liu, Front. Energy Power Eng. 2 (2008) 1–13.
[3] L. Brunel, J. Denele, K. Servat, K.B. Kokoh, C. Jolivalt, C. Innocent, M. Cretin, M. Rolland, S. Tingry, Electrochem. Commun. 9 (2007) 331–336.
[4] S.M. Venkateswara, V. Ilankumaran, N.S. Rao, Indian Pacing Electrophysiol. J. 4 (2004) 201–212.
[5] E. Katz, A.F. Bu¨ckmann, I. Willner, J. Am. Chem. Soc. 123 (2001) 10752–10753.
[6] R.A. Bullen, T.C. Arnot, J.B. Lakeman, F.C. Walsh, Biosens. Bioelectron. 21 (2006) 2015–2045.
[7] C.F. Holmes, J. Power Sources 97–98 (2001) 739–741.
[8] K. Chen, D.R. Merritt, W.G. Howard, C.L. Schmidt, P.M. Skarstad, J. Power Sources 162 (2008) 837–840.
[9] V. Parsonnet, Chest 61 (1972) 165–173.
[10] C.M. Moore, S.D. Minter, R.S. Martin, Lab Chip 5 (2004) 218–225.
[11] L. Akers, C.M. Moore, S.D. Minteer, Electrochim. Acta 50 (2005) 2521–2525.
[12] A. Heller, Phys. Chem. Chem. Phys. 6 (2004) 209–216.
[13] C. Picioreanu, I.M. Head, K.P. Katuri, M.C.M.V. Loosdrecht, K. Scott, Water Res. 41 (2007) 2921–2940.
[14] P.V. Bernhardt, Aust. J. Chem. 59 (2006) 233–256.
[15] M. Madou, Fundamentals of Microfabrication: The Science of Miniaturization, 2nd ed., CRC Press, 2002.
[16] C. Kleinstreuer, Biofluid Dynamics, 2005, Raleigh.
[17] N. Mano, V. Soukharev, A. Heller, J. Phys. Chem. B 110 (2006) 11180–11187.

[18] G.W. Albin, T.A. Horbett, S.R. Miller, N.L. Ricker, J. Control. Rel. 6 (1987) 267–291.
[19] H. Li, R. Luo, E. Birgersson, K.Y. Lam, J. Mech. Phys. Solids 57 (2009) 369–382.
[20] G.K. Kouassi, J. Irudayaraj, G. McCarty, BioMagn. Res. Technol. 3 (2005) 1–10.
[21] J. Cutnell, K. Johnson, Physics, 4th ed., Wiley, New York, 1998.
[22] G.R. Daniel, Physics: Health and the Humanbody, Wadsworth, 1980.
[23] J. Wang, Chem. Rev. 108 (2008) 814–825.
[24] L.J. Appel, M.W. Brands, S.R. Daniels, N. Karanja, P.J. Elmer, F.M. Sacks, Hypertension 47 (2006) 296–308.
[25] D. Ku, Annu. Rev. Fluid Mech. 29 (1997) 399–434.
[26] A. Jafari, S.M. Mousavi, P. Kolari, Commun. Nonlinear Sci. Numer. Simul. 13 (2008) 1615–1626.
[27] B.M. Johnston, P.R. Johnston, S. Corney, D. Kilpatrick, J. Biomech. 39 (2006) 1116–1128.
[28] P.R. Wheater, H.G. Burkitt, V.G. Daniels, Wheater's Functional Histology: A Text and Color Atlas, 1st ed., Churchill Livingstone, New York, 1979.